An Optimal Over-frequency Generator Tripping Strategy for Regional Power Grid with High Penetration Level of Renewable Energy

Zhihang Zhou, Libao Shi, and Yixuan Chen

***Abstract*—This paper proposes an optimal over-frequency generator tripping strategy aiming at implementing the least amount of generator tripping for the regional power grid with high penetration level of wind/photovoltaic (PV), to handle the over-frequency problem in the sending-end power grid under large disturbances. A steady-state frequency abnormal index is defined to measure the degrees of generator over-tripping and under-tripping, and a transient frequency abnormal index is presented to assess the system abnormal frequency effect during the transient process, which reflects the frequency security margin during the generator tripping process. The scenario-based analysis method combined with the non-parametric kernel density estimation method is applied to model the uncertainty of the outgoing power caused by the stochastic fluctuations of wind/PV power and loads. Furthermore, an improved fireworks algorithm is utilized for the solution of the proposed optimization model. Finally, the simulations are performed on a real-sized regional power grid in Southern China to verify the effectiveness and adaptability of the proposed model and method.**

***Index Terms*—Frequency response, over-frequency generator tripping, wind power, photovoltaic (PV), fireworks algorithm.**

I. Introduction

IT is generally known that the system frequency in a power grid reflects the real-time balance of the active power between the supply side and the demand side [1]. As a consequence, the system frequency will deviate following a fault such as the tripping of the main transmission line. When the unbalanced power exceeds the acceptable regulation limit of the system, the conventional frequency regulation effects of loads and generators fail to prevent the continuous system frequency excursion [2]-[4], and several emergency control measures including the over-frequency generator tripping (OFGT) [5]-[8] and the under-frequency load shedding (UFLS) [9]-[13] will be triggered to rebalance the active power between the supply side and the demand side by tripping generators or shedding loads.

In recent years, the rapid development of large-scale grid-connected renewable energy sources has posed huge challenges to the power system dynamics involving voltage stability, transient stability and frequency stability [14]-[17]. These non-synchronous generation units lower the system inertia and make the system frequency response capability worse, which lead to the frequency variation and excursion at a relatively alarming rate when a fault occurs. On August 9, 2019, there was a large power outage accident in the UK that affected nearly 1 million people. The lack of system inertia caused by the high penetration level of renewable energy weakens the system ability to withstand active power disturbances, and on the other hand, it is one of the main reasons to trigger the UFLS protection during faults [18]. In China, there exists higher penetration level of renewable energy in some regional sending-end power grids, and the high frequency problem becomes more serious owing to the unbalanced power in the case of a fault. Therefore, it is imperative to conduct in-depth exploration and exploitation on how to efficiently formulate the OFGT strategy with high penetration level of renewable energy.

To date, the vast majority of the research on the emergency control under a disturbance has mainly focused on the UFLS strategy for the receiving-end power grid, whereas there have been relatively few studies discussing the OFGT strategy for the sending-end power grid. As one of the most important emergency protection measures to alleviate the power surplus in the sending-end power grid, the OFGT strategy can effectively prevent accidents from evolving into a blackout and ensure the safety of the system at the cost of tripping a small number of units in the initial stage of the fault. The capacity of generators to be tripped and the appropriate tripping rounds of the stage-by-stage OFGT strategy are discussed in [6] based on the single-machine equivalent load model. In [7], the configuration principle of the OFGT strategy for multiple circuits of the ultra-high voltage direct current (UHVDC) transmission blocking faults is analyzed, and the OFGT strategy is proposed correspondingly. In addition, in [8], the system frequency characteristics considering the high penetration level of renewable energy are studied. The advantages of tripping the conventional generation unit

Manuscript received: June 14, 2020; accepted: March 2, 2021. Date of Cross-Check: March 2, 2021. Date of online publication: July 27, 2021.

This work was supported in part by the National Natural Science Foundation of China (No. 51777103).

Z. Zhou and L. Shi (corresponding author) are with the National Key Laboratory of Power Systems in Shenzhen, Shenzhen International Graduate School, Tsinghua University, Shenzhen 518055, China (e-mail: zzx18@mails.tsinghua.edu.cn; shilb@sz.tsinghua.edu.cn).

Y. Chen is with the Planning Research Center of Yunnan Power Grid Co., Ltd., Kunming 650051, China (e-mail: chenyx@163.com).

DOI: 10.35833/MPCE.2020.000374

and the renewable energy source with the same capacity for the OFGT strategy are discussed as well. However, most existing OFGT strategies are developed more or less based on the engineering experience. Furthermore, it is not clarified how to set the specific generators to be tripped in each round of OFGT, which needs to be studied further.

This paper proposes an optimal OFGT strategy to discuss the impact of high penetration level of wind/photovoltaic (PV) generation units on system frequency characteristics of the regional sending-end power grid. The scenario-based analysis method is applied to deal with the uncertainties of renewable energy generation, and an improved fireworks algorithm is applied for the solution of the proposed optimization model. The case studies are performed on a real-sized regional power grid in Southern China to verify the validity of the proposed model and method. The main contributions of this paper are summarized as follows.

1) We propose an optimal OFGT model to suppress the system frequency deviation and avoid the frequency collapse under faults with minimum generator tripping cost.

2) We define a steady-state frequency abnormal index (SFAI) and introduce it as a penalty term into the objective function to avoid the risk of generator over-tripping and under-tripping. Furthermore, we propose a transient frequency abnormal index (TFAI) to implement the quantitative evaluation of the system abnormal frequency effect during the transient period under a fault.

3) We adopt the non-parametric kernel density estimation method to model the uncertainty of the outgoing power caused by the uncertainty of renewable energy. And we improve the fireworks algorithm to avoid falling into the local optimal solution when solving the proposed optimization model.

The remainder of this paper is shown as follows. In Section II, the effect of the high penetration level of renewable energy on the frequency characteristics is evaluated, and an optimal OFGT model is established. The solution of the proposed optimization model based on the improved fireworks algorithm combined with the scenario-based analysis method is described in Section III. In Section IV, the case studies are performed on a real-sized regional power grid in Southern China. The conclusions are summarized in Section V.

II. Problem Formulation

A. Frequency Characteristics of Aggregated System Frequency Response (ASFR) Model

In this paper, an ASFR model [19] is applied to analyze the frequency response process of the system under a disturbance. Figure 1(a) shows the block diagram of the ASFR model, where H is the equivalent system inertia constant, D is the damping factor including the generator damping and the load frequency response, R is the frequency droop coefficient, F_H, T_R, T_C, T_G, and K_G are the high-pressure turbine constant, the reheater time constant, the steam chest time constant, the governor time constant, and the mechanical power gain, respectively. The forward link represents the equation of motion of the system equivalent generator, and the feedback loops describe the responses of generators to the frequency variation Δf. When the initial unbalanced power ΔP_{S0} occurs in the system, it is quickly manifested as a system frequency deviation, and this part of the unbalanced power is absorbed by the speed governor action response ΔP_G and the transient surplus power ΔP_S. From Fig. 1(a), the frequency deviation Δf is mainly affected by ΔP_{S0}, R, and H. If ΔP_{S0} is a constant, the transient frequency deviation pertains to the system inertia H, and the larger H is, the smaller the transient frequency deviation is. Similarly, the steady-state frequency deviation is highly correlated to R, and the larger R is, the larger the steady-state frequency deviation is.

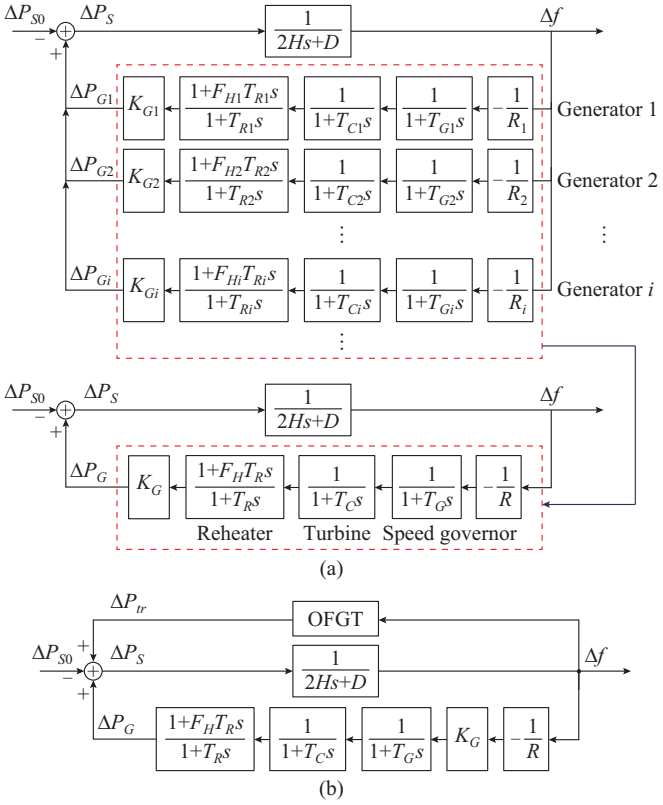

Fig. 1. Block diagram of frequency response process of system. (a) ASFR model. (b) Modified ASFR model with OFGT.

Figure 1(b) shows the block diagram of the modified ASFR model incorporating the OFGT block, where ΔP_{tr} is the total capacity of generators to be tripped. Based on the local frequency information, the stage-by-stage OFGT strategy quickly reduces the redundant power by tripping the generation units when faults occur, thus maintaining the frequency stability of the system.

B. Impact of Grid-connected Renewable Energy Systems on Frequency Response

When the large-scale PV power stations and wind farms are connected to the existing power grid, the frequency response of the system will significantly change owing to the entirely different operation characteristics of the renewable energy generation compared with the conventional power generation. In particular, the changes of the frequency char-

acteristics are primarily reflected in the variations of the frequency droop coefficient and the system inertia constant.

It should be noted that the participation of the renewable energy generation units like wind farms and PV power stations in the frequency regulation is an inevitable trend with increasing penetration level of renewable energy. Some research has been conducted on providing the short-term inertia and supporting the frequency regulation of wind farms [20]-[22]. In a regional power grid, when the installed capacity of the conventional generation units such as hydropower and thermal power units is P_{GC}, and the installed capacity of the renewable energy generation units is P_{GR}, the penetration level of the renewable energy β can be defined as:

$$\beta = \frac{P_{GR}}{P_{GR}+P_{GC}} = \frac{P_{GR}}{P_S} \tag{1}$$

where P_S is the total installed capacity of the system.

To be more specific, if we further differentiate the renewable energy generation units, β can be divided into the following two items: item β_1, which participates in the frequency regulation with improved control strategies, and item β_2 that is not involved in the frequency regulation. Regarding item β_2, for the PV power stations, they have no inertia, and for the wind farms, since they are connected to the power grid via converters, the mechanical system is fully or partially decoupled from the power grid. Therefore, the frequency droop coefficient of the corresponding renewable energy generation R_{GR2} can be perceived as infinity, and the corresponding inertia H_{GR2} is approximated as zero (or very small). We assume that the frequency droop coefficient of the conventional generation system is R_{GC}, and the corresponding inertia constant is H_{GC}. Then the system frequency droop coefficient R_S and the inertia constant H_S with integration of renewable energy can be expressed as:

$$R_S = \frac{\Delta f}{\Delta P} = \frac{\Delta f}{\left(\frac{P_{GC}\Delta f}{R_{GC}} + \frac{P_{GR1}\Delta f}{R_{GR1}} + \frac{P_{GR2}\Delta f}{R_{GR2}}\right)\frac{1}{P_S}} = \frac{1}{\left(\frac{P_{GC}}{R_{GC}} + \frac{P_{GR1}}{R_{GR1}}\right)\frac{1}{P_S}} = \frac{1}{\frac{1-\beta_1-\beta_2}{R_{GC}} + \frac{\beta_1}{R_{GR1}}} \tag{2}$$

$$H_S = \frac{P_{GC}H_{GC}+P_{GR1}H_{GR1}+P_{GR2}H_{GR2}}{P_{GC}+P_{GR}} = \frac{P_{GC}H_{GC}}{P_{GC}+P_{GR}} + \frac{P_{GR1}H_{GR1}}{P_{GC}+P_{GR}} = (1-\beta_1-\beta_2)H_{GC}+\beta_1 H_{GR1} \tag{3}$$

where P_{GR1} is the total power of the renewable energy generation, which contributes to the frequency response and the virtual inertia of the system; P_{GR2} is the rated power of the renewable energy generation without frequency regulation control; H_{GR1} is the equivalent virtual inertia constant; and R_{GR1} is the equivalent droop coefficient.

It should be noted that (2) and (3) have only theoretical significance, because some variables such as R_{GR1} and H_{GR1} are difficult to calculate and may be time dependent [23]. In particular, when all renewable energy generation units do not have the ability of frequency regulation, namely $\beta_1 = 0$, (2) and (3) can be simplified as:

$$R_S = \frac{R_{GC}}{1-\beta} \tag{4}$$

$$H_S = (1-\beta)H_{GC} \tag{5}$$

It can be seen from (4) that the system frequency droop coefficient becomes larger with the integration of wind farms and PV power stations, and the frequency droop coefficient pertinent to the equivalent system R_S increases with the increase of β. As the penetration level of renewable energy increases, the steady-state frequency deviation of the system will eventually become larger. Similarly, it can be seen from (5) that the integration of renewable energy reduces the total inertia of the entire system. Furthermore, as the penetration level of renewable energy increases, the system inertia constant declines, and the frequency deviation in the transient process will further deteriorate according to Fig. 1(a). Therefore, for the regional power grid with the high penetration level of renewable energy, the system frequency would tend to be jeopardized in some extreme faults, and some emergency protection measures such as OFGT should be applied.

C. Optimization Model of OFGT

As the critical stability control measures for the sending-end power system in China, the primary frequency control, the secondary frequency response based on automatic generation control, and the OFGT strategy play significant roles in maintaining the system frequency stability under disturbances. However, the activations of the primary and secondary frequency control require relatively long periods of time, and the regulation capacity is limited [24]. In case of emergency, it is necessary to trip power generation units through OFGT strategy in an attempt to greatly reduce the unbalanced power.

As shown in Fig. 2, when the frequency f rises above the predefined threshold for a period of time (usually 0.1-0.5 s delay time to prevent malfunction), the stage-by-stage OFGT control and processing unit is triggered based on the local frequency, and the tripping signal is sent to the generation side. However, the variation of system operation conditions and the randomness of system failures will weaken the adaptability of the OFGT strategy to a certain extent. In addition, once the OFGT strategy is set up, it will remain unchanged for a long time. Therefore, an effective OFGT strategy should meet the system stability requirements under various operation conditions at the lowest possible generator tripping cost.

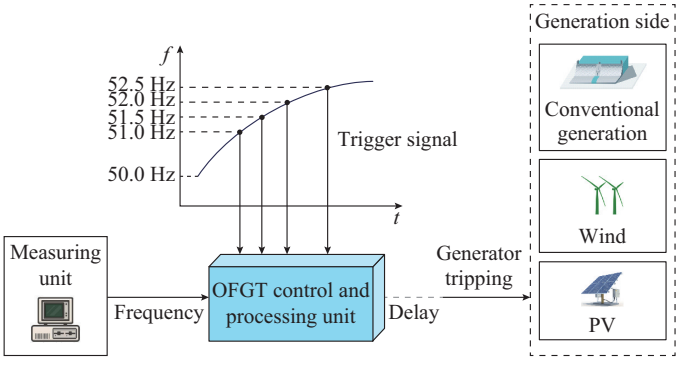

Fig. 2. Schematic diagram of stage-by-stage OFGT strategy.

In this paper, we propose an optimal OFGT model that aims to minimize the generator tripping cost while satisfying a series of system constraints. In the proposed optimization model, the generator tripping cost is represented by the sum of generator capacities tripped for each round, and the corresponding objective function F can be modeled as:

$$\min F=\sum_{i\in N}w_i\sum_{j\in M}\lambda_j\left(\sum_{t\in K}\sum_{l\in L}\mu_{t,l}^{i,j}P_{tr,l}^{i,j}+\left|\Delta P_p^{i,j}\right|+\Delta P_f^{i,j}\right) \tag{6}$$

where w_i is the probability of the i^{th} fault type; λ_j is the probability of the j^{th} typical scenario; N and M are the sets of faults and typical scenarios, respectively; K is the set of generator tripping rounds; L is the set of power generation units including the wind/PV generation units; $\mu_{t,l}^{i,j}$ is a binary variable indicating whether the unit is tripped or not; $P_{tr,l}^{i,j}$ is the generator capacity to be tripped correspondingly; and $\Delta P_p^{i,j}$ and $\Delta P_f^{i,j}$ are the penalty terms pertinent to the steady-state and transient frequencies, respectively, which are described in detail as follows.

1) The penalty term $\Delta P_p^{i,j}$ is defined as a SFAI in this paper, aiming to avoid possible generator over-tripping and under-tripping. The expression of SFAI $\Delta P_p^{i,j}$ is expressed as:

$$SFAI=\Delta P_p^{i,j}=\begin{cases}C_1(f_{fin}-f_{up}) & f_{fin}\geq f_{up}\\ 0 & f_{lo}<f_{fin}<f_{up}\\ C_2(f_{fin}-f_{lo}) & f_{fin}\leq f_{lo}\end{cases} \tag{7}$$

where C_1 is the under-tripping coefficient, whose physical meaning is to convert the excessive steady-state frequency into the under-tripping generator power corresponding to the ideal OFGT strategy; C_2 is the over-tripping coefficient, whose physical meaning is to convert the deficient steady-state frequency into the over-tripping generator power corresponding to the ideal OFGT strategy; f_{fin} is the steady-state frequency after generator tripping; f_{lo} and f_{up} are the lower and upper bounds of the normal allowable steady-state frequency, respectively, such as 49.8-50.2 Hz prescribed for the power grids in China.

The physical meaning of *SFAI* is to measure the degree of generator over-tripping and under-tripping in the OFGT strategy from the perspective of steady-state frequency. According to (7), the value of *SFAI* is mainly determined by the steady-state frequency f_{fin}, and the value range of *SFAI* is $(-\infty, +\infty)$. In our work, $SFAI>0$ denotes the generator under-tripping condition, namely f_{fin} is greater than the upper bound of the allowable steady-state frequency, and the larger the *SFAI* value is, the higher the degree of generator under-tripping is; $SFAI<0$ denotes the generator over-tripping condition, namely f_{fin} is less than the lower bound of the allowable steady-state frequency, and the smaller the *SFAI* value is, the higher the degree of generator over-tripping is; $SFAI=0$ denotes the appropriate generator tripping condition, namely f_{fin} is within the allowable range after the OFGT operation. In addition, the values of C_1 and C_2 are related to the installed capacity of generators and the regulation capability of the system. Their values should not be too small or too large, and need to be designed according to specific application examples.

2) We assume that the transient frequency abnormal duration t_r is the time when the transient frequency exceeds the permitted threshold f_p, in which the corresponding allowable time of equipment is t_p. In order to avoid the adverse influence of high frequency on the turbine blades and satisfy the transient frequency standards of the grid-connection technology for wind and PV power generation, t_r should be less than t_p after the operation of OFGT. Compared with the two-element table method [25] consisting of specific frequency and time, the evaluation method based on frequency integration [26] can better reflect the impact of the cumulative characteristics of transient frequency on system security. Therefore, in this paper, the frequency integration based method is modified to quantitatively evaluate the system abnormal frequency effect during the transient period, and we define the following *TFAI*:

$$TFAI=\frac{\int_{t_s}^{t_s+t_p}(f-f_p)\mathrm{d}t}{(f_p-f_n)t_p} \tag{8}$$

where f_n is the rated frequency of power system; and t_s is the starting time for calculating *TFAI* and can be determined according to (9).

$$f(t_s)=f(t_s+t_p) \tag{9}$$

where $f(t_s)$ and $f(t_s+t_p)$ are the transient frequency values at time t_s and time t_s+t_p within the oscillation range of the maximum transient frequency, respectively.

Furthermore, according to the values of t_r and t_p, Fig. 3 shows three cases of calculating *TFAI*, and *TFAI* can be expressed by the areas of the shaded parts S_1, S_2, S_3 and S_4 as shown in Fig. 3. Therefore, *TFAI* can be expressed as:

$$TFAI=\begin{cases}\dfrac{S_2}{S_1} & t_r\geq t_p\\ \dfrac{S_2-S_3-S_4}{S_1+S_3+S_4} & 0<t_r<t_p\\ -\dfrac{S_2}{S_1+S_2} & t_r=0\end{cases} \tag{10}$$

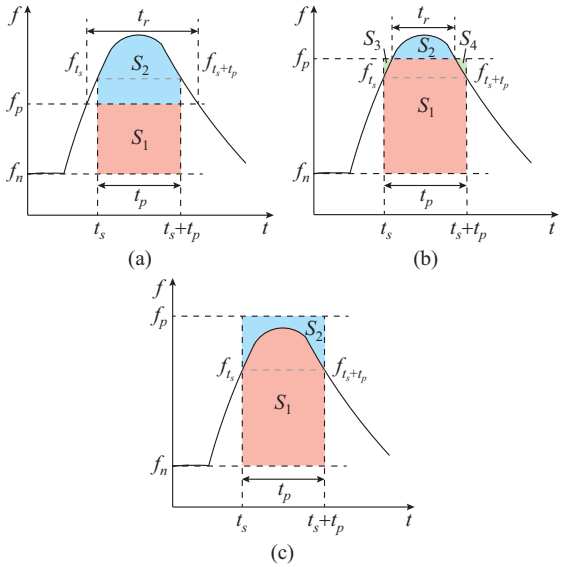

Fig. 3. Transient frequency curves. (a) $t_r\geq t_p$. (b) $0<t_r<t_p$. (c) $t_r=0$.

The physical meaning of *TFAI* denotes the degree of generator under-tripping in the OFGT strategy from the perspective of transient frequency. According to (8) and (10), the value of *TFAI* is mainly determined by the transient frequency f, and the value range of *TFAI* is $[-1, +\infty)$. Here, $TFAI > 0$ indicates that the generator under-tripping occurs, and the larger the value of *TFAI* is, the higher the degree of generator under-tripping is; $TFAI \le 0$ indicates that the transient frequency meets the transient frequency requirements after the OFGT operation. Therefore, the transient frequency penalty term $\Delta P_f^{i,j}$ can be defined as:

$$\Delta P_f^{i,j} = \begin{cases} C_3 \cdot TFAI & TFAI > 0 \\ 0 & TFAI \le 0 \end{cases} \tag{11}$$

where C_3 is the transient frequency penalty coefficient.

The physical meaning of C_3 is to convert the degree of generator under-tripping of OFGT into the under-tripping generator power corresponding to the ideal OFGT strategy from the perspective of transient frequency. Similar to C_1 and C_2, the value of C_3 is related to the installed capacity of generators, the regulation capability of the system, and the preference for transient frequency index and steady-state frequency index in the objective function F. And the value of C_3 needs to be designed according to specific application examples.

The proposed OFGT strategy should also satisfy the following constraints.

1) The tripping generator amount in each round should not be too large or too small:

$$\Delta P_{t,\min} \le \sum_{l \in L} \mu_{t,l}^{i,j} P_{tr,l}^{i,j} \le \Delta P_{t,\max} \tag{12}$$

where $\Delta P_{t,\min}$ and $\Delta P_{t,\max}$ are the minimum and maximum allowed tripping generator amounts in the t^{th} round, respectively.

2) In order to prevent the action of UFLS, the transient frequency f should be more than a certain value after OFGT:

$$f > f_{\min} \tag{13}$$

where $f_{\min}$ is the minimum frequency allowed in the transient process, namely the frequency pertinent to UFLS in the first round.

3) For the regional power grid, when a fault occurs on the external transmission line, and then the regional power grid is disconnected from the main network, the outgoing power P_{out} transmitted to the main network in the normal state can be approximately equal to the initial unbalanced power ΔP_{S0}. Therefore, the transient frequency can be calculated according to Fig. 1(b), and the corresponding equality constraints are given as:

$$P_{out} = P_R + P_C - P_{load} - P_{loss} \tag{14}$$

$$2H \frac{\mathrm{d}\Delta f}{\mathrm{d}t} = P_{out} - \Delta P_{tr} - \Delta P_G - D\Delta f \tag{15}$$

where P_R is the renewable energy generation output; P_C is the conventional power station output; P_{load} is the load power; and P_{loss} is the power loss of the regional power grid.

III. Solution Method

In our work, the scenario-based analysis method is applied to handle the uncertainties caused by wind/PV power generation. Regarding the nonlinear characteristics of the proposed optimization model, it is difficult to solve the model by using the conventional mathematical programming approaches. Therefore, an improved fireworks algorithm is developed for the solution of the proposed optimization model.

A. Scenario-based Analysis Solution

The uncertainties of the renewable energy on the supply side and the load variation over time on the demand side make the operation state of the entire system change constantly. Therefore, P_{out} also fluctuates invariably, which affects the system frequency deviation in turn when a fault occurs on the external transmission line. In practice, the data on the right side of (14) is often known in a certain period of time. If the regularity of the outgoing power P_{out} can be extracted from these samples, a probability model can be established to describe the random variation of the power output that reflects different time periods. As one of the widely used probability density estimation methods, the nonparametric kernel density estimation does not require any prior knowledge and assumptions of the distribution type, which has been successfully used in load sampling for security-constrained unit commitment problems [27]. In this paper, the Gaussian kernel $K(\cdot)$ is used as the kernel function to estimate the probability density function (PDF) $f_d(P_{out})$ of the outgoing power P_{out}, and the corresponding expression is given as:

$$f_d(P_{out}) = \frac{1}{nh} \sum_{i=1}^{n} K\left(\frac{P_{out} - P_{out,i}}{h}\right) \tag{16}$$

where $P_{out,i}$ is the i^{th} sample of the random variable P_{out}; n is the total number of samples; and h is the optimal bandwidth which can be calculated in accordance with [28].

In order to further simulate the uncertainty of P_{out}, a scenario generation technique based on the Wasserstein distance is introduced in the process of converting the continuous PDF into deterministic discrete quantiles Z_w $(w = 1, 2, \ldots, W)$. Z_w can be calculated according to (17) with the minimum distance from the generated scenarios to the initial distribution [29].

$$\int_{-\infty}^{Z_w} (f_d(P_{out}))^{\frac{1}{r+1}} \mathrm{d}P_{out} = \frac{2w-1}{2W} \int_{-\infty}^{+\infty} (f_d(P_{out}))^{\frac{1}{r+1}} \mathrm{d}P_{out} \tag{17}$$

where r is the order of Wasserstein distance; and W is the total number of discrete quantiles.

In addition, the probability λ_w pertinent to quantile Z_w can be described as:

$$\begin{cases} \lambda_0 = \displaystyle\int_{Z_0}^{\frac{Z_0+Z_1}{2}} f_d(P_{out}) \mathrm{d}P_{out} \\ \lambda_w = \displaystyle\int_{\frac{Z_{w-1}+Z_w}{2}}^{\frac{Z_w+Z_{w+1}}{2}} f_d(P_{out}) \mathrm{d}P_{out} \quad w = 1, 2, \ldots, W \\ \lambda_{W+1} = \displaystyle\int_{\frac{Z_W+Z_{W+1}}{2}}^{Z_{W+1}} f_d(P_{out}) \mathrm{d}P_{out} \end{cases} \tag{18}$$

where Z_0 and Z_{W+1} are the upper and lower bounds of P_{out}, respectively.

B. Improved Fireworks Algorithm

In our work, a novel swarm intelligence algorithm, called fireworks algorithm [30], is applied for the solution of the proposed optimization model. The procedure of the fireworks algorithm can be divided into four steps: initialization, explosion, mutation, and selection. In order to improve the global search ability and the optimization speed of the fireworks algorithm, some effective measures are taken, and the details are described as follows.

In the mutation step, a kind of differential mutation [31] is used to replace the original Gaussian variation to improve the convergence speed. We suppose that x_i^k denotes the k^{th} dimension value of fireworks x_i, d represents the differential coefficient, and x_{d1}^k, x_{d2}^k are the k^{th} dimension values of two individuals randomly selected from the difference set. Only when the generated random number is greater than the differential probability, the differential mutation operation is performed as:

$$x_i^k = x_i^k + d(x_{d1}^k - x_{d2}^k) \tag{19}$$

In addition, the optimal solution trimming method [32] is also introduced to avoid local optimality in this mutation step, which performs Gaussian mutation for each component of the current optimal solution sequentially while keeping remaining dimensions unchanged.

In the selection step, the original distance-based selection method is replaced by the elitism random selection [33] to speed up the selection process.

The entire flow chart for the solution of the proposed optimization model is shown in Fig. 4.

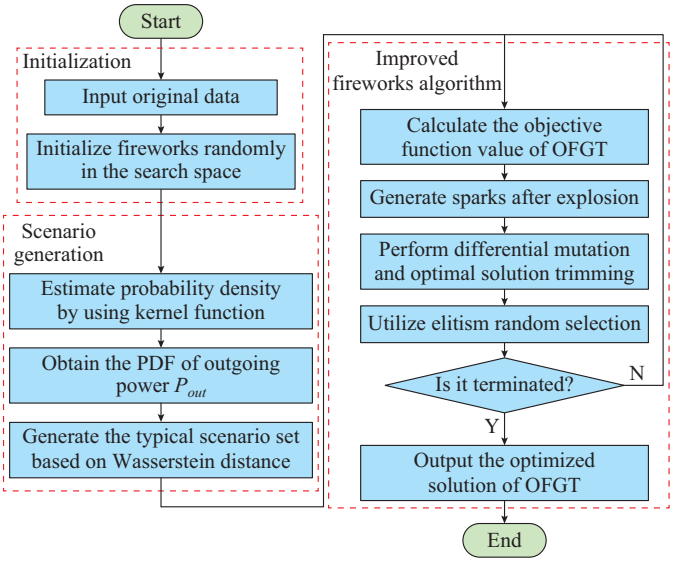

Fig. 4. Flow chart of improved fireworks algorithm for solution of proposed OFGT optimization model.

IV. Case Study

A real-sized regional power grid in Southern China is tested to validate the effectiveness of the proposed optimization model in BPA and MATLAB simulation environments. The geographical diagram of the regional power grid is shown in Fig. 5. By the end of 2020, it is estimated that, in the region, there will be eleven hydropower plants with 209 MW installed capacity, nine PV power stations with 247 MW installed capacity, and three wind farms with 343 MW installed capacity. Therefore, the penetration level of the renewable energy will increase, up to 74%. Under the typical operation conditions, the hydropower plants have the output of 209 MW, and the regional load power consumption is 358 MW. If the simultaneity factor which is introduced to assess the coincidence of renewable energy generation output is taken as 0.5, the renewable energy generation output will account for 59% of total power output, and the power loss of the regional power grid is 14 MW. Therefore, the total 132 MW outgoing power will be transmitted to the main network through the main transformer.

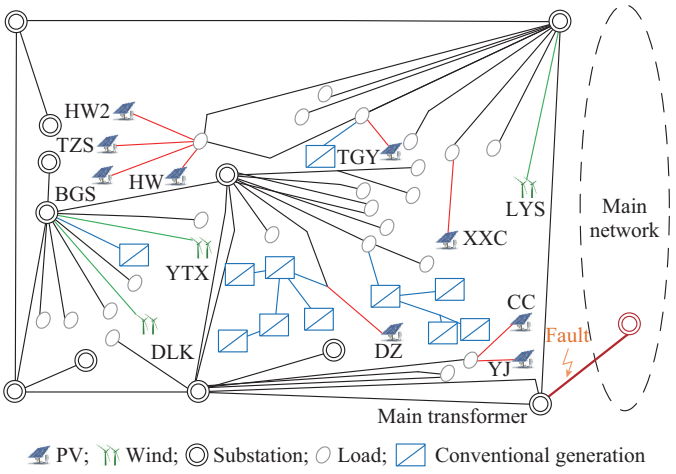

Fig. 5. Geographical diagram of regional power grid in Southern China with wind/PV integration.

In addition, Fig. 6 shows the daily power curves of the PV power station output, the wind farm output, the load demand power and the outgoing power to the main network, respectively. This regional power grid has the typical characteristics of the sending-end power grid with wind/PV integration.

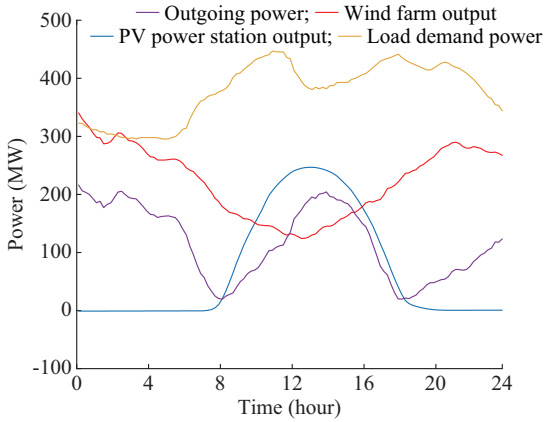

Fig. 6. Daily power curves in regional power grid.

A. Frequency Response Characteristics of Renewable Energy

As shown in Fig. 5, when the line pilot protection operates under a short-circuit fault on the outgoing transmission

line between the main transformer and the main network, the regional power grid is separated from the main network and forms an isolated network. The voltage curves of PV power stations and wind farms at the point of common coupling (PCC) are shown in Appendix A Fig. A1 and Fig. A2. According to the grid code technical rules relevant to the zero/low voltage ride-through for grid-connected wind farms and PV power stations as given in Appendix A Fig. A3 and Fig. A4 [34], [35], all the PV power stations and wind farms can operate continuously without disconnecting from the power grid within a certain voltage drop range in a time interval. In addition, at this time, the frequency of the isolated network rises rapidly without taking any control and protection measures, and the output power curves of different types of power generation units under a fault are shown in Fig. 7(a).

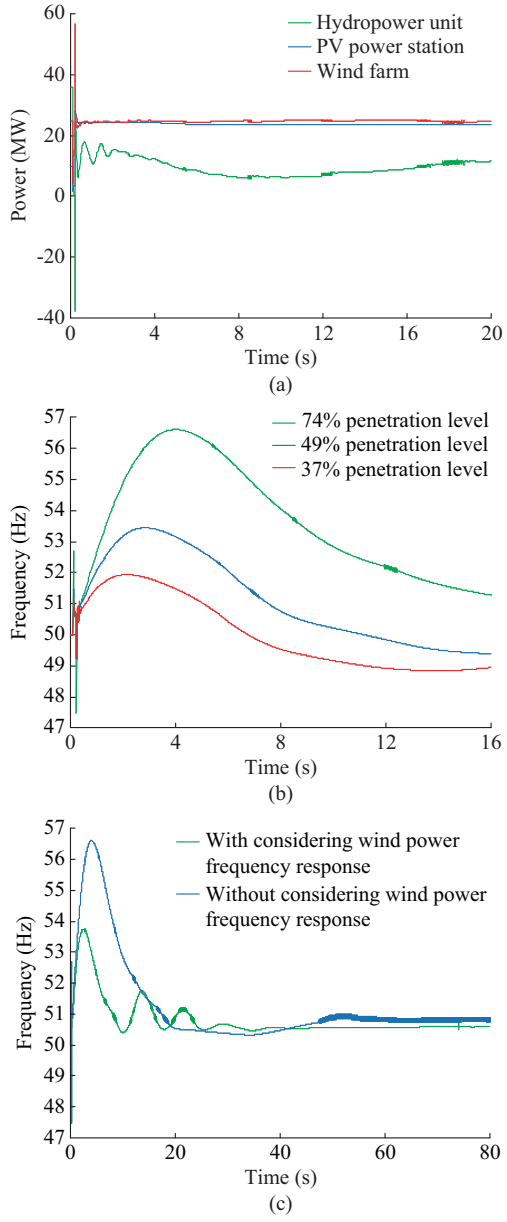

Fig. 7. Output power variations and frequency deviations under a fault. (a) Output power variations. (b) Frequency deviations with different wind/PV penetration levels. (c) Comparison of system frequency excursion with/without considering wind power frequency response.

It can be seen that the hydropower unit constantly regulates the outputs to adapt to the increase or decrease of the system frequency, while the wind farm output and the PV power station output remain constant when the frequency changes. To study the impact of renewable energy penetration on the system frequency characteristics under the fault, the equivalent variation of the wind and the penetration level of PV is realized by replacing the wind turbine with a hydropower unit with the same capacity, as shown in Fig. 7(b). It can be seen that the system frequency characteristic is gradually deteriorating, and the transient maximum frequency is also rising with the increase of the penetration level of renewable energy. In particular, when the system frequency changes, the wind farms and the PV power stations no longer participate in the frequency response. As mentioned above, the large-scale grid-connected wind farms and PV power stations significantly reduce the system inertia. Therefore, the frequency characteristic of the system becomes worse, and the frequency deviation gets larger under the large disturbance. In this paper, the comparison of the system frequency excursion with and without considering the wind power frequency response is shown in Fig. 7(c), and the wind farm frequency control strategy is utilized in accordance with [36]. It can be seen that the participation of renewable energy in frequency control can be positive to restrain the increase of the transient frequency under a fault, however, the effect on the restoration of the steady-state frequency is relatively small due to the apparently limited regulation capacity.

B. Simulation Results of Optimal OFGT Strategy

Compared with tripping the conventional generation units, tripping the renewable energy generation units has obvious advantages in maintaining system inertia and reducing tripping capacity [8]. Therefore, the renewable energy generation units are set to be tripped in the prior round of the stage-by-stage OFGT strategy for the regional power grid, and the conventional generation units will be tripped in subsequent rounds if the wind and PV generation capacities are not enough. According to the grid code technical rules for grid-connected wind farms and PV power stations to participate in the OFGT strategy in a provincial power grid of China, when the grid frequency exceeds 51.5 Hz, the wind farm is requested to sustain the operation for at least 5 min. However, the PV power station is allowed to be disconnected from the power grid. Therefore, the ability of the PV power station to withstand the high frequency is weaker than that of the wind farm, and the PV power station should be tripped firstly. Additionally, in order to ensure the protection coordination of two kinds of OFGT strategies between the provincial main network and the regional grid, the OFGT strategy for the regional power grid should not be activated during the OFGT operation for the main network. As a consequence, the starting frequency of the OFGT for the regional gird should be greater than the final value of the OFGT for the provincial main network, namely 51.4 Hz. In this paper, the PV power station is taken as the target to be tripped in the first round of the OFGT strategy with operation fre-

quency at 51.5 Hz, and the wind farm is selected as the target to be tripped in the second round of the OFGT strategy with operation frequency at 52 Hz. However, in the third round, the hydropower unit is not required to be set in the OFGT strategy of the regional power grid because the load demands are always greater than the hydropower outputs. Therefore, the over-frequency deviation can be suppressed only by tripping some renewable units in the first and second rounds. Furthermore, the delay time of each round takes the empirical value of 0.1 s in this paper. The coefficients C_1 and C_2 given in (7) are both set to be 2000 MW/Hz, and the coefficient C_3 given in (11) is set to be 70 MW. The number of fireworks is set to be 20, and the explosion constant and mutation constant are set to be 20 and 5, respectively.

Figure 8 shows the comparison between the continuous PDF and the discrete probability density of the typical scenario pertinent to the outgoing power based on Section III-A. It should be noted that, in this paper, the discrete probability density is defined as the discrete probability divided by the length between quantiles of different scenarios to make sense. The probability values of $\lambda_j (j=0,1,2,3,4,5)$ given in (18) pertinent to these discrete scenarios are 0.133, 0.187, 0.177, 0.156, 0.218, and 0.129, respectively. It can be seen that there is a good match between the contour of the discrete probability density and the continuous PDF as shown in Fig. 8. Therefore, the typical scenario generation based on the Wasserstein distance adequately describes the stochastic fluctuation characteristics of the initial PDF, and provides a feasible way to model the uncertainty of outgoing power caused by the uncertainty of wind/PV power generation.

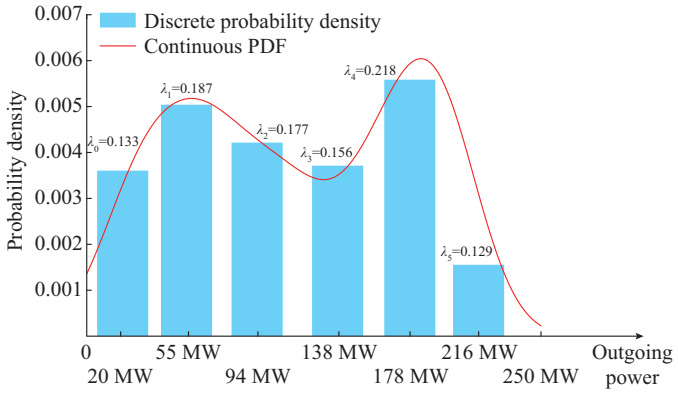

Fig. 8. Contour of discrete probability density and continuous PDF of outgoing power.

The detailed results of the proposed optimal OFGT strategy in each round are listed in Table I. The total generator tripping capacity is 206.5 MW, including 70 MW PV power tripped in the first round and 136.5 MW wind power tripped in the second round. In order to check the adaptability of the proposed optimal OFGT strategy, the same short-circuit fault occurring on the outgoing transmission line is applied in the following six typical extreme cases.

1) Case 1: maximum load conditions with 99.6 MW outgoing power.

2) Case 2: minimum load conditions with 161 MW outgoing power.

3) Case 3: maximum PV power output conditions with 191 MW outgoing power.

4) Case 4: maximum wind power output conditions with 213 MW outgoing power.

5) Case 5: maximum outgoing power conditions which are identical with Case 4.

6) Case 6: minimum outgoing power conditions with 20.5 MW outgoing power.

TABLE I
GENERATOR TRIPPING SET IN EACH ROUND

Round	Operation frequency (Hz)	Delay time (s)	Tripping set	Capacity (MW)
1	51.5	0.1	DZ, XXC, TGY	70.0
2	52.0	0.1	LYS-1G, DLK-1G, LYS-2G	136.5

The corresponding simulation results are shown in Table II. It can be seen from Table II that the steady-state frequencies of all modes are stable close to 50 Hz and meet the frequency fluctuation requirements under normal operation conditions. It should be noted that the generator tripping capacity in Case 6 is zero because the redundant power under the fault is so small that the transient maximum system frequency has not yet reached the OFGT action value of the first round. Furthermore, Fig. 9 illustrates the frequency response characteristics when tripping the wind/PV generation units and the conventional generation units with the same capacity in Case 2. As expected, the steady-state frequency approaches to 50 Hz when applying the proposed strategy, while the steady-state frequency reaches 50.9 Hz when tripping the conventional generation units.

TABLE II
SIMULATION RESULTS IN EXTREME CASES

Case	Generator tripping capacity (MW)	Steady-state frequency (Hz)
1	60.2	50.06
2	102.4	50.06
3	121.9	50.07
4	136.5	50.06
5	136.5	50.06
6	0	50.02

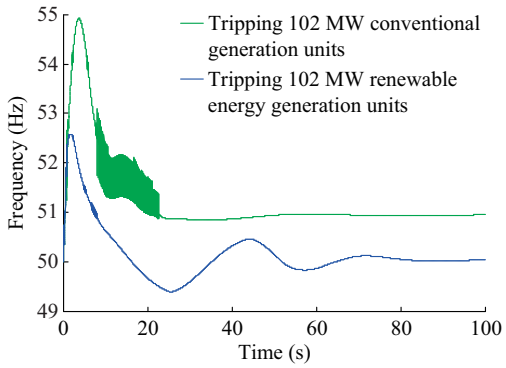

Fig. 9. Comparison of frequency response characteristics when tripping different types of generation units in Case 2.

C. Comparative Analysis

In order to achieve sustainable power generation on the premise of giving priority to renewable energy, the conventional generation units are usually tripped in the OFGT strategy to avoid tripping wind and PV generation units. In this paper, a traditional OFGT strategy incorporating the conventional generation units for the regional grid is applied to compare with the proposed optimal OFGT strategy. In the traditional OFGT strategy, the capacity of generators to be tripped in each round is determined by the steady-state frequency just at the upper bound of the allowable steady-state frequency (namely 50.2 Hz) after the action of OFGT. However, the consequence of tripping the conventional generation units based on the traditional method in the prior rounds causes the system inertia to gradually decrease and is not conducive to the system stability. The peak value of the transient frequency increases correspondingly, and the subsequent rounds of the OFGT strategy may be triggered incorrectly, resulting in a generator over-tripping problem. In particular, the continuous high and low frequency oscillations in the configuration process of OFGT make the traditional method difficult to implement, as shown in Fig. 10.

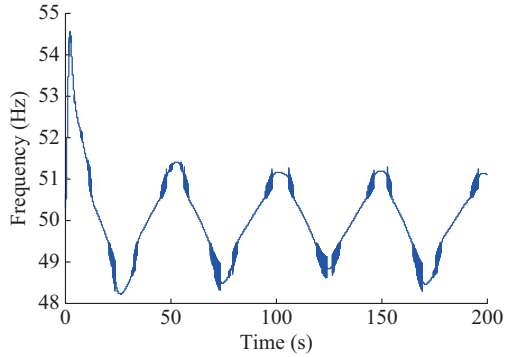

Fig. 10. High and low frequency oscillations in configuration process of OFGT when using traditional method.

V. Conclusion

The high penetration level of renewable energy in the regional power grid causes the system frequency characteristics to deteriorate owing to the low inertia and the lack of frequency response following a fault. In this paper, an optimal OFGT strategy with the least amount of generator tripping incorporating renewable energy is proposed to suppress the system frequency deviation and prevent frequency collapse under large disturbances. The scenario-based analysis method is introduced to model the uncertainty of outgoing power caused by wind/PV generation uncertainties, and an improved fireworks algorithm is applied to solve the proposed optimization model. Finally, the simulations performed on a real-sized regional power grid in Southern China validate the effectiveness of the proposed model and method. The results show that the proposed optimal OFGT strategy can effectively sustain system frequency stability and be well adapted to various operation conditions. Compared with tripping conventional generation units, tripping wind/PV generation units in the prior rounds of OFGT strategy is better in stabilizing frequency under a fault.

Appendix A

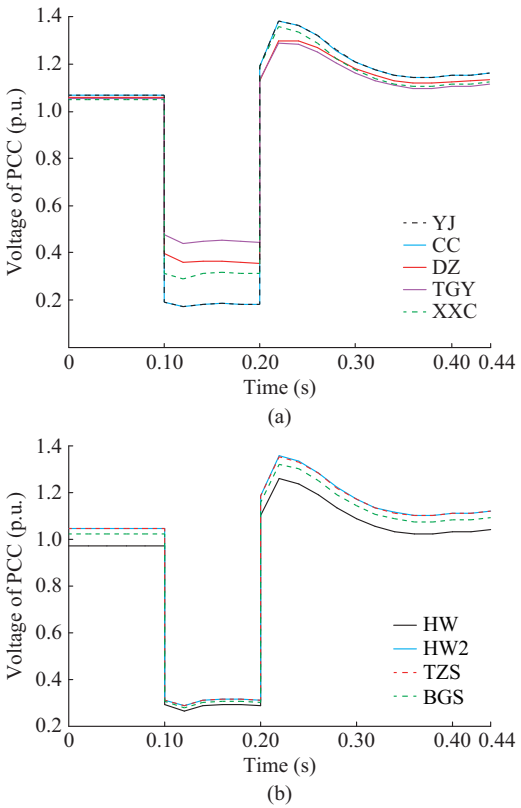

Fig. A1. Voltage curves at PCC of PV power stations. (a) Voltage curves at PCC of PV power stations YJ, CC, DZ, TGY, and XXC. (b) Voltage curves at PCC of PV power stations HW, HW2, TZS, and BGS.

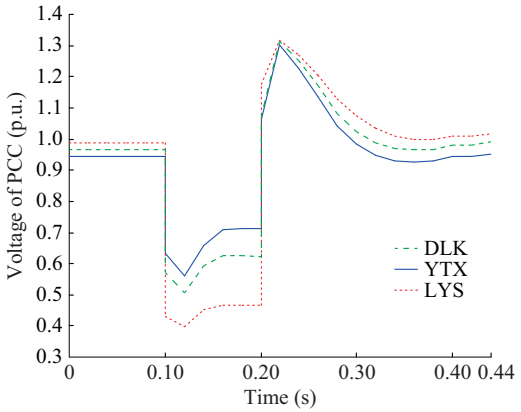

Fig. A2. Voltage curves at PCC of wind farms DLK, YTX, and LYS.

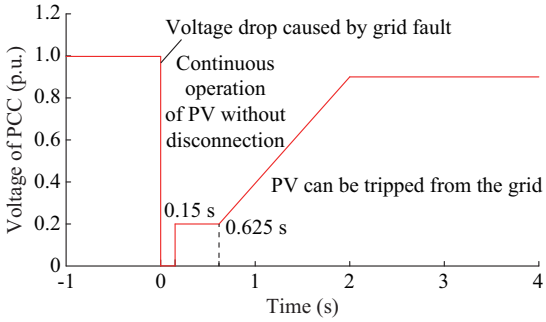

Fig. A3. Zero voltage ride-through standard for PV power station.

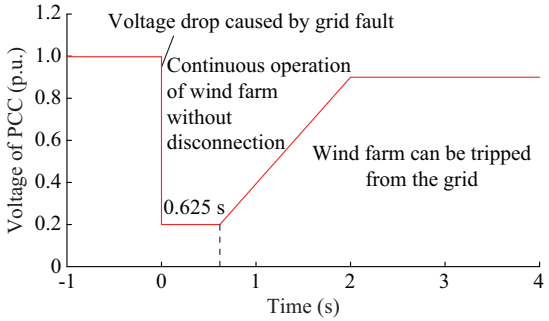

Fig. A4. Low voltage ride-through standard for wind farm.

REFERENCES

[1] Y. Bian, H. Wyman-Pain, F. Li *et al*., "Demand side contributions for system inertia in the GB power system," *IEEE Transactions on Power Systems*, vol. 33, no. 4, pp. 3521-3530, Jul. 2018.

[2] Y. Kim, L. K. Norford, and J. L. Kirtley, "Modeling and analysis of a variable speed heat pump for frequency regulation through direct load control," *IEEE Transactions on Power Systems*, vol. 30, no. 1, pp. 397-408, Jan. 2015.

[3] J. Hu, J. Cao, J. M. Guerrero *et al*., "Improving frequency stability based on distributed control of multiple load aggregators," *IEEE Transactions on Smart Grid*, vol. 8, no. 4, pp. 1553-1567, Jul. 2017.

[4] Q. Shi, F. Li, G. Liu *et al*., "Thermostatic load control for system frequency regulation considering daily demand profile and progressive recovery," *IEEE Transactions on Smart Grid*, vol. 10, no. 6, pp. 6259-6270, Nov. 2019.

[5] Z. Song, Y. Lin, C. Liu *et al*., "Review on over-frequency generator tripping for frequency stability control," in *Proceedings of IEEE PES Asia-Pacific Power and Energy Engineering Conference*, Xi'an, China, Oct. 2016, pp. 2240-2243.

[6] Z. Zhang, Y. Xu, R. Yuan *et al*., "Frequency characteristics of power grid at sending end of split large-scale interconnected regional power grid and corresponding over-frequency generator-tripping scheme," *Power System Technology*, vol. 39, no. 1, pp. 288-293, Jan. 2015.

[7] Z. Zhang, R. Yuan, Y. Xu *et al*., "Optimization of over-frequency generator-tripping scheme in Sichuan power grid adaptable to multi-UHVDC transmission project," *Automation of Electric Power Systems*, vol. 40, no. 2, pp. 141-146, Jan. 2016.

[8] Y. Chen, D. Chen, Y. Wang *et al*., "Studies on high-frequency generator tripping strategy for sending system of wind-PV-thermal-bundled power transmitted by HVDC," in *Proceedings of International Conference on Renewable Power Generation*, Beijing, China, Oct. 2015, pp. 1-6.

[9] W. Gu, W. Liu, J. Zhu *et al*., "Adaptive decentralized under-frequency load shedding for islanded smart distribution networks," *IEEE Transactions on Sustainable Energy*, vol. 5, no. 3, pp. 886-895, Jul. 2014.

[10] B. Potel, V. Debusschere, F. Cadoux *et al*., "A real-time adjustment of conventional under-frequency load shedding thresholds," *IEEE Transactions on Power Delivery*, vol. 34, no. 6, pp. 2272-2274, Dec. 2019.

[11] S. S. Banijamali and T. Amraee, "Semi-adaptive setting of under frequency load shedding relays considering credible generation outage scenarios," *IEEE Transactions on Power Delivery*, vol. 34, no. 3, pp. 1098-1108, Jun. 2019.

[12] J. A. Laghari, H. Mokhlis, M. Karimi *et al*., "A new under-frequency load shedding technique based on combination of fixed and random priority of loads for smart grid applications," *IEEE Transactions on Power Systems*, vol. 30, no. 5, pp. 2507-2515, Sept. 2015.

[13] J. Wang, H. Zhang, and Y. Zhou, "Intelligent under frequency and under voltage load shedding method based on the active participation of smart appliances," *IEEE Transactions on Smart Grid*, vol. 8, no. 1, pp. 353-361, Jan. 2017.

[14] R. Venkatraman, S. K. Khaitan, and V. Ajjarapu, "Impact of distribution generation penetration on power system dynamics considering voltage ride-through requirements," in *Proceedings of IEEE PES General Meeting*, Portland, USA, Aug. 2018, pp. 1-5.

[15] Q. Wang, A. Xue, T. Bi *et al*., "Impact of DFIG-based wind farm on transient stability of single machine infinite bus system," in *Proceedings* of *IEEE PES Asia-Pacific Power and Energy Engineering Conference*, Kowloon, China, Dec. 2013, pp. 1-5.

[16] S. You, Y. Liu, J. Tan *et al*., "Comparative assessment of tactics to improve primary frequency response without curtailing solar output in high photovoltaic interconnection grids," *IEEE Transactions on Sustainable Energy*, vol. 10, no. 2, pp. 718-728, Apr. 2019.

[17] N. A. Masood, N. Modi, T. K. Saha *et al*., "Investigation of non-synchronous penetration level and its impact on frequency response in a wind dominated power system," in *Proceedings of IEEE PES General Meeting*, Boston, USA, Jul. 2016, pp. 1-5.

[18] National Grid ESO. (2019, Sept.). Technical report on the events of 9 August 2019. [Online]. Available: https://www. nationalgrideso. com/document/152346/download

[19] Q. Shi, F. Li, and H. Cui, "Analytical method to aggregate multi-machine SFR model with applications in power system dynamic studies," *IEEE Transactions on Power Systems*, vol. 33, no. 6, pp. 6355-6367, Nov. 2018.

[20] H. Ye, W. Pei, and Z. Qi, "Analytical modeling of inertial and droop responses from a wind farm for short-term frequency regulation in power systems," *IEEE Transactions on Power Systems*, vol. 31, no. 5, pp. 3414-3423, Sept. 2016.

[21] Y. Tan, K. M. Muttaqi, P. Ciufo *et al*., "Enhanced frequency regulation using multilevel energy storage in remote area power supply systems," *IEEE Transactions on Power Systems*, vol. 34, no. 1, pp. 163-170, Jan. 2019.

[22] G. He, Q. Chen, C. Kang *et al*., "Cooperation of wind power and battery storage to provide frequency regulation in power markets," *IEEE Transactions on Power Systems*, vol. 32, no. 5, pp. 3559-3568, Sept. 2017.

[23] A. F. Guillamón, A. V. Rodríguez, and Á. M. García, "Analysis of power system inertia estimation in high wind power plant integration scenarios," *IET Renewable Power Generation*, vol. 13, no. 15, pp. 2807-2816, Nov. 2019.

[24] P. M. Ashton, C. S. Saunders, G. A. Taylor *et al*., "Inertia estimation of the GB power system using synchrophasor measurements," *IEEE Transactions on Power Systems*, vol. 30, no. 2, pp. 701-709, Mar. 2015.

[25] H. Zhang and Y. Liu, "New index for frequency deviation security assessment," in *Proceedings of IPEC*, Singapore, Singapore, Oct. 2010, pp. 1031-1034.

[26] J. Dai, Y. Tang, and Q. Wang, "Fast method to estimate maximum penetration level of wind power considering frequency cumulative effect," *IET Generation, Transmission & Distribution*, vol. 13, no. 9, pp. 1726-1733, Jun. 2019.

[27] D. Lu, Z. Bao, and Z. Li, "Load sampling for SCUC based on principal component analysis and kernel density estimation," in *Proceedings of IEEE PES General Meeting*, Boston, USA, Jul. 2016, pp. 1-5.

[28] Z. Lu, X. Xu, Z. Yan *et al*., "Density-based global sensitivity analysis of islanded microgrid loadability considering distributed energy resource integration," *Journal of Modern Power Systems and Clean Energy*, vol. 8, no. 1, pp. 94-101, Jan. 2020.

[29] Q. Wang, W. Dong, and L. Yang, "A wind power/photovoltaic typical scenario set generation algorithm based on Wasserstein distance metric and revised K-medoids cluster," *Proceedings of the CSEE*, vol. 35, no. 11, pp. 2654-2661, Jun. 2015.

[30] S. Zheng, A. Janecek, and Y. Tan, "Enhanced fireworks algorithm," in *Proceedings of IEEE Congress on Evolutionary Computation*, Cancun, Mexico, Jun. 2013, pp. 2069-2077.

[31] C. Yu, L. Kelley, S. Zheng *et al*., "Fireworks algorithm with differential mutation for solving the CEC 2014 competition problems," in *Proceedings of IEEE Congress on Evolutionary Computation*, Beijing, China, Jul. 2014, pp. 3238-3245.

[32] Z. Zhou, L. Shi, X. Xu *et al*., "Multi-objective distribution network reconfiguration with DG integration using improved fireworks algorithm," in *Proceedings of International Conference on Renewable Power Generation*, Shanghai, China, Oct. 2019, pp. 1-8.

[33] S. Zheng, A. Janecek, J. Li *et al*., "Dynamic search in fireworks algorithm," in *Proceedings of IEEE Congress on Evolutionary Computation*, Beijing, China, Jul. 2014, pp. 3222-3229.

[34] *Technical Requirements for Connecting Photovoltaic Power Station to Power System*, China Standard GB/T 19964-2012, 2012.

[35] *Technical Rule for Connecting Wind Farm to Power System*, China Standard GB/T 19963-2011, 2011.

[36] K. Clark, N. W. Miller, and J. J. Sanchez-Gasca, "Modeling of GE wind turbine-generators for grid studies," General Electric International, Inc., Schenectady, NY, Tech. Rep. Apr. 2010.

Zhihang Zhou received the B. E. degree in electrical engineering from North China Electric Power University, Baoding, China, in 2018. He is currently pursuing the M.E. degree with the National Key Laboratory of Power

Systems in Shenzhen, Shenzhen International Graduate School, Tsinghua University, Shenzhen, China. His research interests include power system cascading failure and emergency control.

Libao Shi received the B.S., M.Sc., and Ph.D. degrees from the Department of Electrical Engineering, Chongqing University, Chongqing, China, in 1994, 1997, and 2000, respectively. He was a Postdoctoral Research Associate at The University of Hong Kong, Hong Kong, China, from August 2004 to June 2006. He is currently an Associate Professor with the National Key Laboratory of Power Systems in Shenzhen, Shenzhen International Graduate School, Tsinghua University, Shenzhen, China. His research interests include complementary and coordinated dispatch technologies with multi-energy source structure, cyber-physical power systems, power system cascading failure, and restoration control.

Yixuan Chen received the B.E. and M.E. degrees from Southwest Jiaotong University, Chengdu, China, in 2006 and 2009, respectively, both in electrical engineering. He is now a Senior Engineer at Planning Research Center of Yunnan Power Grid Co., Ltd., Kunming, China. His research interests include power system protection and emergency control.